Weakly nonlinear optimal perturbations

Jan O. Pralits, Alessandro Bottaro, Stefania Cherubini

Weakly nonlinear optimal perturbations

JAN O. PRALITS[1]†, ALESSANDRO BOTTARO[1] and STEFANIA CHERUBINI[2]

[1]DICCA, Università di Genova, Via Montallegro 1, 16145 Genova, Italy
[2] DynFluid, Arts et Metiers ParisTech, 151, Bd. de l'Hôpital, 75013 Paris, France

A simple approach is described for computing spatially extended, weakly nonlinear optimal disturbances, apt at maintaining a disturbance-regeneration cycle in a simple shear flow. Weakly nonlinear optimals, computed over a short time interval for the expansion used to remain tenable, are oblique waves which display a shorter streamwise and a longer spanwise wavelength than their linear counterparts. Threshold values of the initial excitation energy, separating the region of damped waves from that where disturbances grow without bounds, are found. Weakly nonlinear optimal solutions of varying initial amplitudes are then fed as initial conditions to direct numerical simulations of the Navier-Stokes equations and it is shown that the weakly nonlinear model permits to identify flow states which cause rapid breakdown to turbulence.

1. Introduction

Optimal perturbations represent a fundamental concept of the linear stability theory of shear flows and one highly cited textbook (Schmid & Henningson 2001) centers much of the discussion on this concept and on the associated idea of transient growth of disturbances for systems ruled by non-normal linear operators. It has been thought for quite some time that, under nominally stable conditions, the most dangerous initial disturbances computed in a linear setting might undergo a substantial amplification, eventually capable of bringing the fluid system outside of the domain of attraction of the laminar solution (and also outside of the domain of validity of the linearized equations), so that transition can occur because of nonlinear interactions. This has provided the rationale for studying linear optimal disturbances, via a number of approaches including eigenfunction expansion (Butler & Farrell 1992), expansion in periodic functions (Criminale *et al.* 1997) and adjoint equations (Andersson *et al.* 1999; Luchini 2000; Corbett & Bottaro 2001).

Linear, optimal perturbations in simple parallel shear flows, such as Couette, Poiseuille or Hagen-Poiseuille flows, take the form of streamwise or quasi-streamwise vortices (the streamwise wavenumber α either vanishes or is very small, in the latter case decreasing like Re^{-1}, with Re the Reynolds number), and their downstream evolution turns them into spanwise-periodic streaks, elongated along the main flow direction, x. While the presence of vortices and streaks seems appropriate in view of experimental observations of transitional flow features, their very early presence in the flow field is unwarranted since $x-$invariant flow structures trigger nonlinear interactions very slowly and only when their amplitude is large, through the onset and growth of a traveling wave instability (Andersson *et al.* 2001; Gustavsson 2009).

The traditional concept of optimal disturbances (those which give rise to the largest

† Email address for correspondence: jan.pralits@unige.it

disturbance energy growth over a given time window, or over a given spatial development length, should one consider flows developing in space) is thus misleading if one searches for the initial waveform most suited to provoke transition, at least for the simplest shear flows. This has been understood for a few years now, and has produced a rising number of contributions on non-linear optimals (Zuccher *et al.* 2006; Cherubini *et al.* 2011; Cherubini & De Palma 2013; Pringle & Kerswell 2010; Monokrousos *et al.* 2011; Pringle *et al.* 2012; Rabin *et al.* 2012; Duguet *et al.* 2013) which have highlighted the profound differences between linear and nonlinear transient growth. In the abstract of their contribution Rabin *et al.* (2012) state that all of their results "highlight the irrelevance of the linear energy gain optimal perturbation for predicting or describing the lowest-energy flow structure which triggers turbulence." Nonlinear optimals are typically found via adjoint looping (Luchini & Bottaro 2014) and are very demanding in terms of computer memory and CPU time, because of the need to carry out several direct simulations of the Navier-Stokes equations and to store (or recompute, via a checkpointing procedure) the whole flow field at all times for use in the adjoint equations. Thus, a thorough parametric search (in terms of wavenumbers, disturbance amplitude and target time of the optimization) is still out of reach.

A weakly nonlinear alternative, much cheaper computationally than the full nonlinear optimization approach, is explored in the present paper. The approach pursued aims at identifying initial perturbations which distort efficiently – via primary nonlinear interactions – the main flow. It will be shown that such optimal solutions take the form of oblique structures. It has been known since Schmid & Henningson (1992) that the early appearance of oblique waves elicits faster transition than either optimal streamwise vortices or Tollmien-Schlichting waves (see also Schmid & Henningson, 2001). The mechanism described by Schmid & Henningson (1992) has been called *oblique transition*; they have expressed the generic disturbance field, ϕ, in Fouries series, e.g.

$$\phi(x,y,z,t) = \sum_{m=-M}^{M} \sum_{n=-N}^{N} \tilde{\phi}_{m,n}(y,t) e^{i(m\alpha x + n\beta z)},$$

where x, y and z indicate, respectively, the streamwise, wall-normal and spanwise direction; α and β are the streamwise and spanwise wavenumbers; M and N are positive integers that define the truncation of their direct numerical simulation. By imposing at $t = 0$ a disturbance field in the form of a pair of oblique waves with $(m, n) = (1, \pm 1)$, Schmid & Henningson (1992) have observed a rapid amplification of the mean flow distortion, mode $(0, 0)$, accompanied by a growth (equally rapid but less vigorous) of the streamwise-independent component, $(0, \pm 2)$; conversely, the $(\pm 2, 0)$ mode remained an order of magnitude smaller. The $(0, \pm 2)$ component is ruled by a nonnormal evolution operator, very sensitive to external forcing, and can thus be enhanced linearly by a transient growth mechanism, yielding large amplitude streaks via the lift-up effect (Landahl 1975). Much attention has been paid to the instability of such streaks, with lower emphasis placed on the fact that the streaks develop on top of a base flow which is being strongly distorted. The predominance of the $(0, 0)$ non-linearly generated component, even above the $(1, \pm 1)$ mode, is, however, evident in figs. 1 and 2 of the paper by Schmid & Henningson (1992). It is thus clear the interest of studying the optimal linear (modal or nonmodal) growth of an oblique disturbance developing over a base flow which is being deformed nonlinearly by the primary wave itself. This calls for an autonomous cycle, schematized in fig. 1, with the first generation of non-linear interactions (the Reynolds stresses), which feeds onto the mean flow. The present paper describes the simplest possible model of such a cycle: the creation of harmonics, past the $(0, 0)$ mode which concentrates in itself the

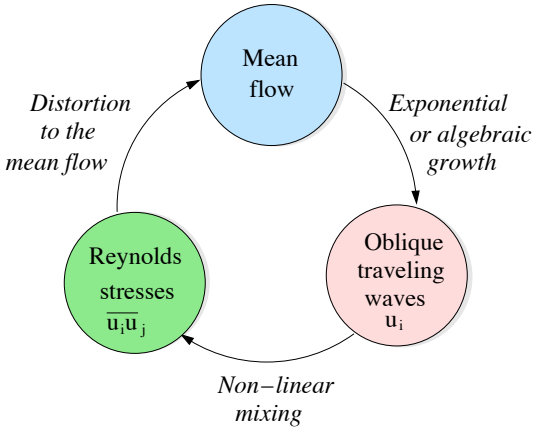

FIGURE 1. Self-sustaining cycle centered on the optimal amplification of oblique waves.

majority of growth, is neglected. We thus study the rapid transient growth of an oblique wave and search for that optimal initial disturbance capable of creating and maintaining the self-sustained, neutral cycle sketched in fig. 1. The appropriateness of the present *minimal model* will be demonstrated by comparisons with direct numerical simulations.

2. Formulation of the weakly non-linear problem

A self-sustained cycle can be created decomposing velocity and pressure into a steady, laminar parallel state, a traveling wave and a slowly varying time-dependent base flow distortion. The idea for this decomposition stems from Biau & Bottaro (2009); however, other papers in the recent literature (Hall & Sherwin 2010; Blackburn *et al.* 2013; Beaume *et al.* 2015) have also split the disturbance field in a streamwise-invariant (i.e. mean) and a streamwise-varying (i.e. fluctuations) component, reaching a set of equations in which the Reynolds stresses force the growth of the mean flow. The decomposition employed here assumes no *a priori* scaling on the Reynolds number and reads:

$$\begin{bmatrix} U(y) \\ 0 \\ 0 \\ P(x) \end{bmatrix} + \epsilon \begin{bmatrix} \tilde{u}(x,y,z,t) \\ \tilde{v}(x,y,z,t) \\ \tilde{w}(x,y,z,t) \\ \tilde{p}(x,y,z,t) \end{bmatrix} + \epsilon^2 \begin{bmatrix} u_{00}(y,t) \\ v_{00}(y,t) \\ w_{00}(y,t) \\ p_{00}(y,t) \end{bmatrix}, \tag{2.1}$$

where $\epsilon \in \mathbb{R}$ denotes the wave amplitude. In the following, the simplest wall-bounded flow is considered but the procedure is general and can easily be applied to semi-infinite or infinite domains. The $\mathcal{O}(\epsilon)$ terms correspond to the traveling wave which we wish to optimize for; those of $\mathcal{O}(\epsilon^2)$ are the mean flow distortion terms which dominate the nonlinear interactions at early times. Clearly the decomposition proposed is insufficient at large times when higher modes are created and interact; it is however adequate, as we will show, to approximate the lower bound of the amplitude ϵ beyond which the flow can undergo transition to turbulence. The flow decomposition (2.1) is introduced into the Navier-Stokes equations and like-order terms are collected. At order $\mathcal{O}(1)$ we obtain

$$P_x = \frac{1}{Re} U_{yy}, \tag{2.2}$$

with subscripts denoting partial differentiation, plus no-slip boundary conditions for U. The Reynolds number, Re, is based on the half-channel thickness and the wall velocity. For the case of the Couette flow treated here P is constant and $U = y$, for $y \in [-1, 1]$. The disturbance at $\mathcal{O}(\epsilon)$ is taken to be a simple monochromatic wave which travels along a direction inclined by $tan^{-1}(\beta/\alpha)$ with respect to the x-axis:

$$(\tilde{\mathbf{u}}, \tilde{p})(x, y, z, t) = (\mathbf{u}_{11}, p_{11})(y, t)e^{i(\alpha x+\beta z)} + (\mathbf{u_{11}}^*, p_{11}^*)(y, t)e^{-i(\alpha x+\beta z)}, \tag{2.3}$$

where superscript * denotes complex conjugation, $\tilde{\mathbf{u}} = (\tilde{u}, \tilde{v}, \tilde{w})$, and $\alpha, \beta \in \mathbb{R}$ are the streamwise and spanwise wave numbers, respectively. Using expression (2.3), the governing equations, linearized around the perturbed and time-varying mean flow $[U(y) + \epsilon^2\, u_{00}(y, t), 0, \epsilon^2\, w_{00}(y, t)]$, are given by

$$i\alpha u_{11} + v_{11_y} + i\beta w_{11} = 0, \tag{2.4}$$

$$u_{11_t} + i\alpha(U + \epsilon^2\, u_{00})u_{11} + v_{11}(U + \epsilon^2\, u_{00})_y + i\beta(\epsilon^2\, w_{00})u_{11} + i\alpha p_{11} = \frac{1}{Re}\Delta_k u_{11}, \tag{2.5}$$

$$v_{11_t} + i\alpha(U + \epsilon^2\, u_{00})v_{11} + i\beta(\epsilon^2\, w_{00})v_{11} + p_{11_y} = \frac{1}{Re}\Delta_k v_{11}, \tag{2.6}$$

$$w_{11_t} + i\alpha(U + \epsilon^2\, u_{00})w_{11} + v_{11}(\epsilon^2\, w_{00_y}) + i\beta(\epsilon^2\, w_{00})w_{11} + i\beta p_{11} = \frac{1}{Re}\Delta_k w_{11}, \tag{2.7}$$

where $\Delta_k = \partial^2/\partial y^2 - k^2$ and $k^2 = \alpha^2 + \beta^2$. Equations (2.4)-(2.7) are accompanied by no-slip conditions on both the upper and lower walls and an initial condition $\mathbf{u}_{11}(y, t = 0)$ which we will optimize for. At order $\mathcal{O}(\epsilon^2)$ the equations read

$$v_{00} = 0, \tag{2.8}$$

$$u_{00_t} - \frac{1}{Re}u_{00_{yy}} = -[v_{11}u_{11_y}^* + i\beta w_{11}^* u_{11} + c.c.], \tag{2.9}$$

$$p_{00_y} = -[i\alpha u_{11}^* v_{11} + v_{11}v_{11_y}^* + i\beta w_{11}^* v_{11} + c.c.], \tag{2.10}$$

$$w_{00_t} - \frac{1}{Re}w_{00_{yy}} = -[i\alpha u_{11}^* w_{11} + v_{11}w_{11_y}^* + c.c.], \tag{2.11}$$

plus the usual no-slip conditions on both walls. The key point of the analysis is the fact of retaining the x- and $z-$component of the velocity at $\mathcal{O}(\epsilon^2)$ in the expression of the base state above which the mode $(1, 1)$ is superposed (note also that we have anticipated the fact that $v_{00} = 0$ in writing equations 2.5-2.7). The fact of having lifted a higher order term to equations at lower order is motivated by the need to allow for a distorted base state. From the mathematical point of view, this corresponds to replacing the original series (2.1) in powers of ϵ into a sequence of unknown (and decreasing) functions of ϵ (Van Dyke 1975; Cousteix & Mauss 2007). The Orr-Sommerfeld stability equation for the Blasius boundary layer flow is the best-known example of one such instance.

System (2.4)-(2.7) plus equations (2.9) and (2.11) are solved by maximising the energy of the oblique mode at the target time $t = T$, defined as

$$e(T) = \frac{\epsilon^2}{2}\int_{-1}^{1}(u_{11}u_{11}^* + v_{11}v_{11}^* + w_{11}w_{11}^*)dy\Big|_{t=T}. \tag{2.12}$$

Alternative measures of growth could have been considered, for example based on the r.h.s. terms of equations (2.9-2.11). In light of previous experience (e.g., Bottaro *et al.* 2006; Monokrousos *et al.* 2011; Rabin *et al.* 2012), the conclusions reached here would probably be but mildly affected; this remains however to be verified. For assigned ϵ the nonlinear problem is solved iteratively in the following manner:

(a) Maximise the energy $e(T)$, constrained by equations (2.4)-(2.7), over a given time

span T, to find u_{11}, v_{11}, w_{11}. The optimization procedure is performed via adjoint looping; in the first iteration set $u_{00} = w_{00} = 0\ \forall y, t$.

(b) Compute the right hand side of equations (2.9) and (2.11), and solve for $u_{00}(y,t)$ and $w_{00}(y,t)$ under the initial condition $u_{00}(y,0) = w_{00}(y,0) = 0$; equations (2.9) and (2.11) are heat equations with Reynolds stress terms acting as source. Then, go back to (a).

(c) Convergence is declared when the final wave energy $e(T)$ converges to within a defined precision. The normalization employed is $e(0) = \epsilon^2$.

In order to quantify the results, suitable quantities are defined which can also be used in the limit $\epsilon \to 0$ to compare with linear optimal results from the literature. The gain G is

$$G(\epsilon, Re, \alpha, \beta, T) = \frac{e(T)}{e(0)}, \tag{2.13}$$

and is obtained from the converged solution of the procedure outlined above, for given values of α, β, Re and ϵ in a defined temporal interval $[0, T]$. Finally, the mean-flow distortion is quantified by evaluating its "energy":

$$E_U(t) = \frac{\epsilon^4}{4}\int_{-1}^{1} u_{00}^2(y,t)dy \quad \text{and} \quad E_W(t) = \frac{\epsilon^4}{4}\int_{-1}^{1} w_{00}^2(y,t)dy. \tag{2.14}$$

2.1. *Numerical procedure*

The problem outlined at step (a) in the solution procedure is a constrained maximization problem which can be solved using Lagrange multipliers. The governing equations are written in primitive variable form and the resulting adjoint equations are derived using a discrete approach (see Luchini & Bottaro 2014). The spatial derivatives are discretized using second order finite differences and a semi-implicit second-order scheme is used to advance in time. A uniform grid is used in the y-direction and 300 discrete points are sufficient to obtain a converged solution. The code has been tested on several cases found in the literature for $\epsilon \to 0$ (i.e. the mean flow is not distorted); in particular, the value of the optimal gain $\tilde{G} = 0.00118\, Re^2$ and the corresponding time at which it is achieved, $T = 0.117\, Re$, with $\alpha = 35/Re$ and $\beta = 1.60$, are recovered with less than 0.1% error (Schmid & Henningson 2001). Results are obtained imposing that convergence is reached when the relative difference in gain between two consecutive iterations is less than 10^{-8}.

3. Weakly non-linear results

To illustrate results, the case $Re = 400$ is chosen. We take four values of ϵ and fix the wavenumbers α and β as well as the final time T; all parameters selected are given in the caption of figure 2, which displays the curves of gain (equation 2.13) together with the energies of the mean flow modification for the cases in which $\epsilon > 0$. We choose a rather small value of the final time in order to avoid situations in which the nonlinear effects become dominant for which an expansion of the waves including higher harmonics would be necessary.

For $\epsilon < 0.0153$ all solutions are damped for $t > 15$. For $\epsilon \approx 0.0153$ a limit condition is reached, with the different energy measures neither increasing nor decreasing. This corresponds to a threshold between initial disturbance states which relaminarize and states which might lead the flow to turbulence. When $\epsilon > 0.0153$ the measure of energy in figure 2 shows a monotonic increase. We can note that the two components of the energy of the mean flow distortion differ by almost one order of magnitude. This fact might lead to the idea that including the $\epsilon^2 w_{00}$ terms in the wave equations, (2.5)-(2.7), yields a negligible effect. This will be further discussed in section 3.1.

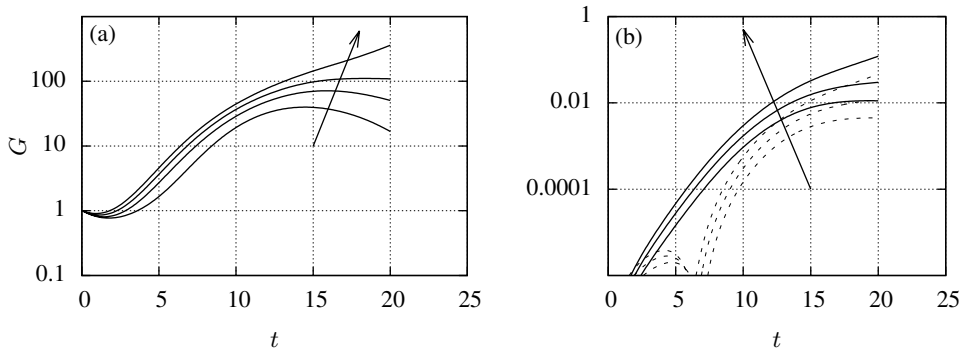

FIGURE 2. (a) Gain G as a function of the final time t for $\epsilon \to 0$, $\epsilon = 0.015, 0.0153, 0.016$, for $\alpha_{opt} = 0.93$, $\beta_{opt} = 1.44$ (obtained by choosing $T = 20$ as target time for the optimization) and $Re = 400$. (b) Energy of the mean flow modification, E_U $(-)$ and E_W $(--)$, for $\epsilon = 0.015, 0.0153, 0.016$. The arrows display increasing values of ϵ.

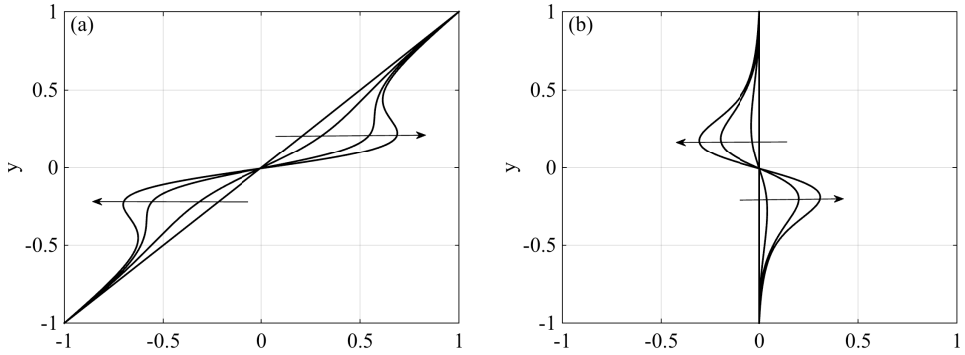

FIGURE 3. Components of the mean flow $U + \epsilon^2 u_{00}$ (a) and $\epsilon^2 w_{00}$ (b) at $t = 0, 10, 15, 20$ for the case $Re = 400$, $\epsilon = 0.0153$, $\alpha_{opt} = 0.93$ and $\beta_{opt} = 1.44$. The arrows display increasing values of t.

Figure 3 shows, for $\epsilon = 0.0153$, the mean flow U and its distortion at $t = 0, 10, 15, 20$, highlighting the presence of an inflection point, in both the streamwise and the spanwise velocity components, at $y = 0$.

The optimal disturbance wave at $t = 0$ is displayed in modulus and phase in figure 4, and through isocontours of u_{11} and (v_{11}, w_{11}) vectors in figure 5. The modulus of the optimal disturbance peaks, both at $t = 0$ and at the target time, in correspondence of the inflection point of the mean flow. The initial perturbation is tilted in the (y, z) plane at $t = 0$, and grows in time developing a slant in the opposite sense, under the forcing of the mean flow distortion shown in figure 3.

Figure 6 displays the gain G at $T = 20$ in the Fourier plane, for four different values of ϵ. For $\epsilon = 0$ the results are those from the classical optimal perturbation theory and the maximum value of G is found for $(\alpha, \beta) = (0.34, 1.72)$. As the value of ϵ exceeds ≈ 0.015 a second region emerges for larger values of α and smaller values of β. This is more evident in figure 6(c) with $\epsilon = 0.0153$, while in figure 6(d) this new peak, with $(\alpha, \beta) = (0.93, 1.44)$, is clearly dominant. If ϵ is further increased (not shown here) the

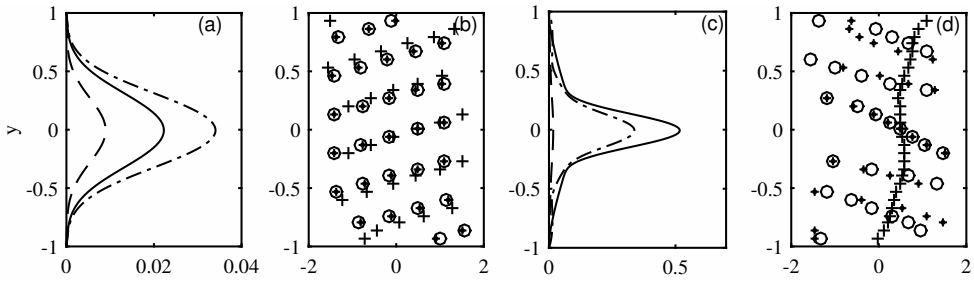

FIGURE 4. Modulus of velocity components and phase of the optimal oblique wave at $t = 0$ (a,b) and its output at the target time $T = 20$ (c,d). The u_{11}, v_{11} and w_{11} components of the velocity are presented in (a,c) as solid, dashed and dash-dotted lines, respectively. The phase, in radians, of the u_{11}, v_{11} and w_{11} components are shown in (b,d) as $\circ$, $+$ and $*$, respectively, and the parameters are those of figure 3.

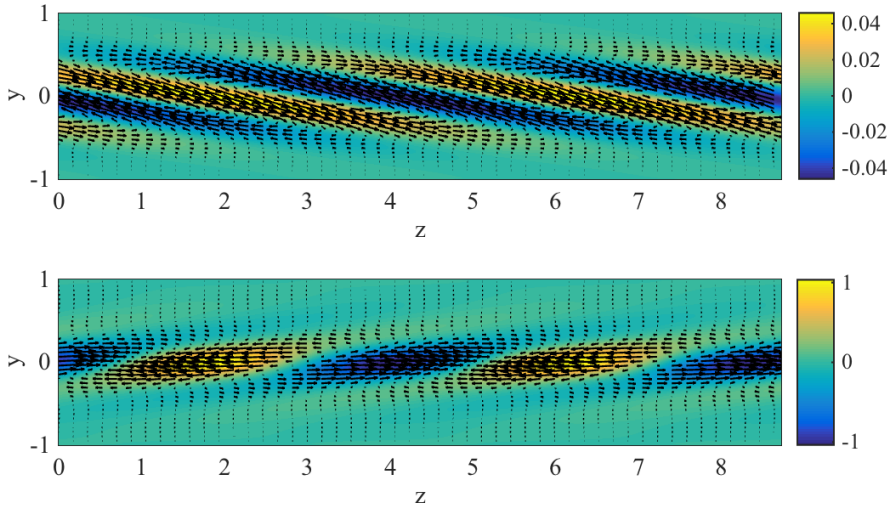

FIGURE 5. Vectors and contours, in the (y, z) plane, of the optimal oblique wave at $t = 0$ (top) and at the target time $T = 20$ (bottom), shown over two spanwise periods. The shaded contours represent the positive and negative streamwise velocity component, whereas the vectors represent wall-normal and spanwise components. Same parameters as in figure 3.

values of α and β, where the peak of G is found, remain at 0.93 and 1.44, respectively. We denote these weakly nonlinear optimal values of the wave numbers as α_{opt} and β_{opt}.

In figure 7(a) we report α_{opt} and β_{opt} for different values of the final time T used in the optimization procedure. For $T < 15$ the streamwise wavenumber is larger than the spanwise wavenumber, in particular at $T = 10$ $\alpha \approx 2\,\beta$. For $T > 15$ the opposite is true and both α_{opt} and β_{opt} have asymptotic behavior for large values of T. In particular the asymptotic value of the spanwise wavenumber approaches its linear counterpart, i.e. 1.60. The value of ϵ which indicates a limit condition is here denoted ϵ_{crit} and its value as a function of the target time T of the optimization is shown in figure 7(b). As one could expect, ϵ_{crit} decreases with T, reaching the asymptotic value $\epsilon_{crit} \approx 0.015$ already for T as low as 30.

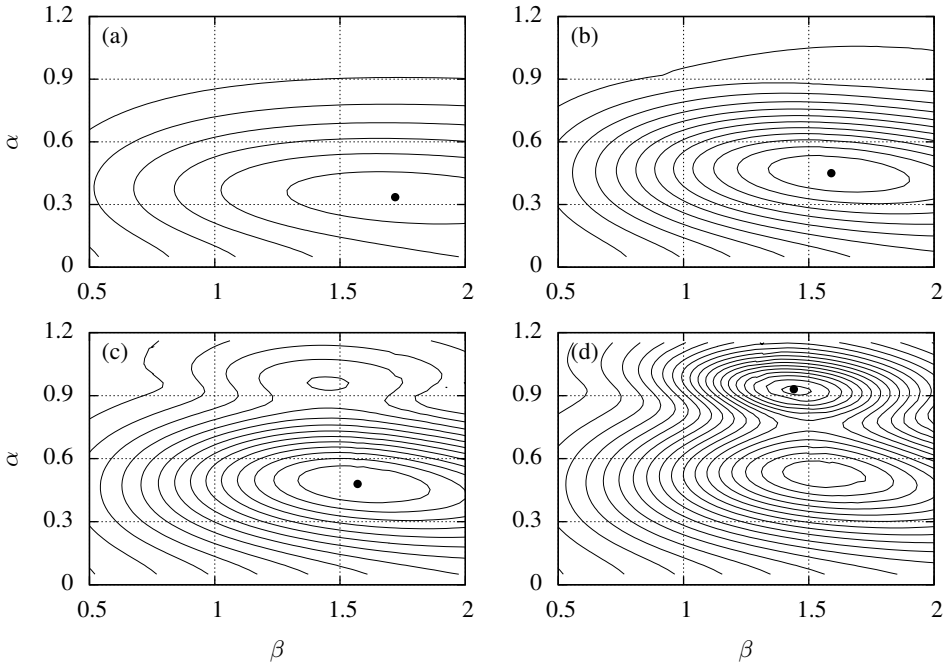

FIGURE 6. Gain G in the $\alpha - \beta$ plane for $Re = 400$ and $T = 20$; (a) $\epsilon \to 0$ with contour values from 20 to 120, (b) $\epsilon = 0.0145$ with contour values from 20 to 240, (c) $\epsilon = 0.0153$ with contour values from 20 to 300, (d) $\epsilon = 0.01603$ with contour values from 20 to 380. The interval among adjacent isolines is ΔG=20 in frames. The maximum value of G for each ϵ is denoted by a filled circle.

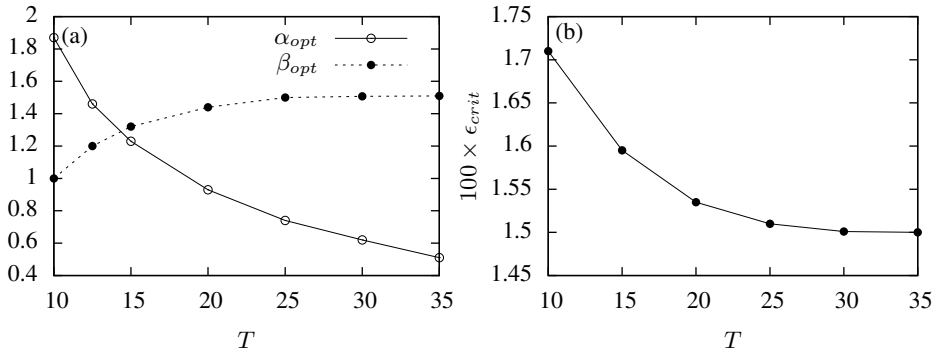

FIGURE 7. (a) Optimal streamwise (α_{opt}) and spanwise (β_{opt}) wavenumbers as a function of T; (b) critical amplitude (ϵ_{crit}) as a function of T. $Re = 400$.

3.1. *Neglecting the correction to the transverse velocity*

In figure 2 is was shown that the measure E_W was about one order of magnitude smaller than E_U. This seems to imply that the mean-flow component w_{00} can be safely omitted from the equations for the optimal oblique disturbance; such an approximation has been made, for example, by Farrell & Ioannou (2012). This is, however, not true – at least in the present model – as the example here will show. Let us consider the case in which $Re = 400$ and the terms $\epsilon^2 w_{00}$ are not included in equations (2.5)–(2.7). The corresponding optimal

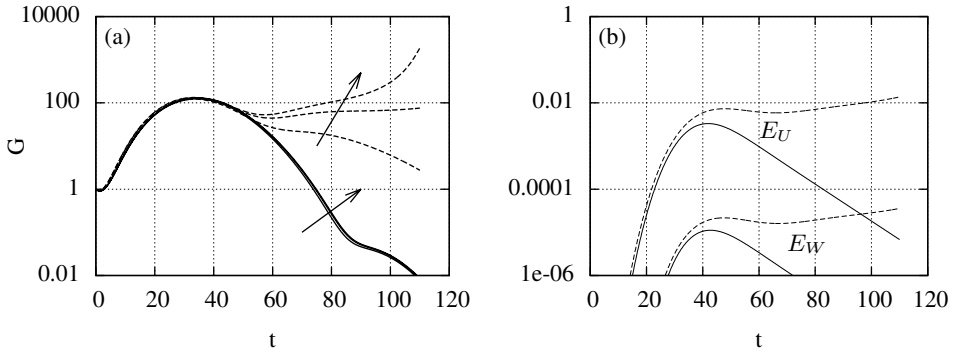

FIGURE 8. (a) Gain G as a function of time t for $\epsilon = 0.0078, 0.0084, 0.0086$, and $\alpha_{opt} = 0.27$, $\beta_{opt} = 1.083$ (obtained in the case excluding the $\epsilon^2 w_{00}$ terms) and $Re = 400$. Lines $(-)$ denote the case including $\epsilon^2 w_{00}$-terms, $(--)$ is the case without the $\epsilon^2 w_{00}$ terms; the arrow displays increasing values of ϵ. (b) Energy of the mean flow modification when $\epsilon = 0.0084$ for both E_U and E_W in the case $(--)$ without $\epsilon^2 w_{00}$ terms and $(-)$ including $\epsilon^2 w_{00}$ terms.

wavenumbers, optimized also with respect to T, are $\alpha_{opt} = 0.27$ and $\beta_{opt} = 1.083$. In figure 8 we report the values of the gain G and energies E_U and E_W for three different values of ϵ. A limiting condition is found for $\epsilon \approx 0.0084$, similar to what shown in figure 2. Here, the value of w_{00} is not included in the governing equations and the value of E_W is only shown for comparison with the value of E_U. Clearly E_W is two orders of magnitude smaller than E_U. If we now include the $\epsilon^2 w_{00}$ terms in (2.5)–(2.7) and compute the gain and energies due to the mean-flow distortion using the values of α_{opt} and β_{opt} previously obtained, no limiting condition is found, and all solutions are damped for $t > 40$ (cf. figure 8 (a), thick solid lines). This holds for all values of ϵ used and also for larger values of ϵ (not shown here).

The result is somewhat unexpected and it confirms that acting on the spanwise mean flow is an efficient strategy to control fluid motion (Gatti & Quadrio 2013).

4. Non-linear results and comparison

The weakly non-linear optimal solutions obtained for $T = 20$, $\alpha_{opt} = 0.93$ and $\beta_{opt} = 1.44$, and different values of ϵ ranging from 0 to 0.016 have been used to initialize several Direct Numerical Simulations (DNSs). The computational domain has length $2\pi/\alpha_{opt}$ in the streamwise direction and $2\pi/\beta_{opt}$ in the spanwise domain. The chosen domain is discretized using a staggered grid and the Navier–Stokes equations are solved by a fractional-step method with second-order accuracy in space and time (Verzicco & Orlandi (1996)). In order to provide a measure of the perturbation energy in the whole computational domain we define two integral energies, E and E_{wavy}, the former based on the whole perturbation, $\mathbf{u}$, and the latter only on its wavy part, $\mathbf{u}_{wavy} = \mathbf{u} - \epsilon^2 \mathbf{u}_{00}$. The perturbation and wavy integral energies are thus defined as:

$$E = \frac{1}{2V} \int_V u^2 + v^2 + w^2 \, dV \qquad E_{wavy} = \frac{1}{2V} \int_V u_{wavy}^2 + v_{wavy}^2 + w_{wavy}^2 \, dV, \tag{4.1}$$

with $V = \frac{8\pi^2}{\alpha_{opt}\beta_{opt}}$ the computational domain. As in the previous section, gains are defined with respect to the energy at the initial time. In particular, the gain G predicted by the weakly non-linear model will be compared with the wavy energy gain, $E_{wavy}(t)/E_{wavy}(0)$ provided by the DNS, which, for brevity, will be labeled G as well. Figure 9 (a) shows

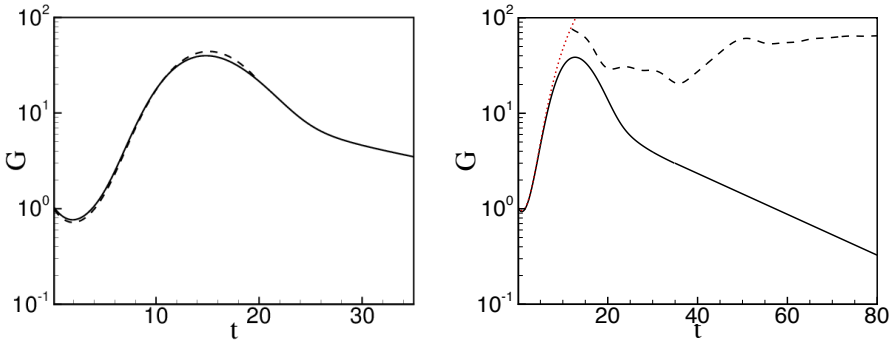

FIGURE 9. (a) Energy gain computed by the weakly non-linear model (dashed line) and by the DNS (solid line) both initialized with the optimal solution obtained at $t = 0$ for $T = 20$, $\epsilon = 0.014$. (b) Energy gain versus time obtained by DNS (black solid line) and by the weakly non-linear model (red dotted line) initialized with the initial optimal solutions for $\epsilon = 0.016$. The black dashed line represent the wavy energy gain for a DNS initialized by the optimal solution extracted at $t = 12$ for the same value of ϵ.

the wavy energy gain obtained by DNS using the initial optimal solution for $\epsilon = 0.014$, compared with that predicted by the weakly non-linear model for the same value of ϵ. The two curves show a remarkable agreement, indicating that the weakly non-linear expansion succeeds in predicting the evolution of the perturbations, provided that non-linear effects are not too strong. On the other hand, for considerably larger values of ϵ (in particular, for $\epsilon > \epsilon_{crit}$), the prediction provided by the weakly non-linear model for $\epsilon = 0.016$, after a finite time (equal to about 10 in figure 9 (b)), begins to differ from the DNS. This can be observed in figure 9 (b) by comparing the red dotted and the solid black curves. This discrepancy is clearly due to the fact that, for large enough amplitudes, non-linear effects become too strong to be correctly approximated by a weakly non-linear expansion. However, despite the differences in energy amplification, the perturbation resulting from the weakly non-linear model is able to induce a self-sustaining cycle leading to turbulence. The dashed line in figure 9 (b) shows that, when the field obtained at $t = 12$ by the model is injected as initial perturbation into the DNS, sudden transition to turbulence is observed. A similar behaviour is observed when using optimal solutions extracted at larger times, provided that the initial value of ϵ is sufficiently large.

To determine the critical value of ϵ for transition to turbulence, we perform several DNSs initializing the computations with fields extracted at $t = 15$; the initial conditions providing the $t = 15$ solutions are the weakly nonlinear optimal disturbances found at different values of ϵ for the same target time, $T = 20$. This choice is motivated by the fact that the energy gain predicted by the model reaches a maximum at approximately $t \approx 15$, as shown, e.g., in figure 9.

Figure 10 shows the integral energy curves obtained by DNS for 4 values of ϵ ranging from 0.0151 to 0.0154. For the lowest value of ϵ the perturbation energy decreases in time, leading the flow to relaminarization. Whereas, for $\epsilon \geqslant 0.0152$, the energy increases reaching a statistically steady value, while the flow is characterized by a chaotic motion. This critical value of ϵ for transition to turbulence, determined by DNS, is very close to the critical one predicted by the model, $\epsilon_{crit} = 0.0153$. This result might have been anticipated, considering that the strong increase of the energy gain observed by the model for $\epsilon > \epsilon_{crit}$ is associated with the development of strong non-linear effects. In

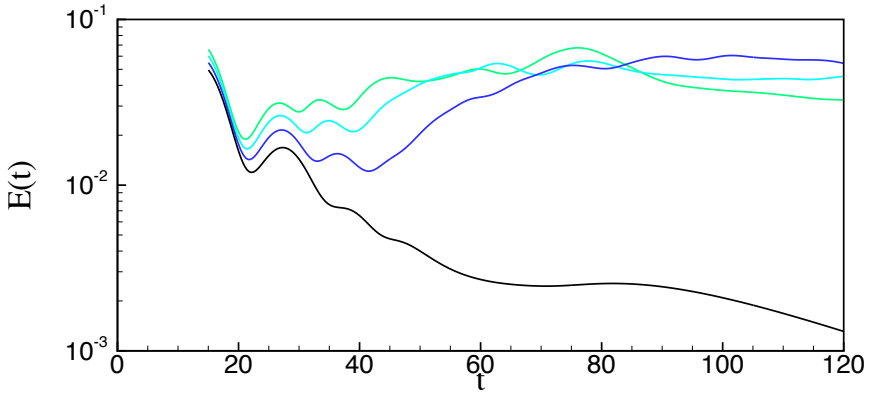

FIGURE 10. Disturbance energy E versus time measured by a DNS initialized with the weakly nonlinear optimal states at $t = 15$, $\epsilon = 0.0151, 0.0152, 0.0153, 0.0154$ (increasing from bottom to top).

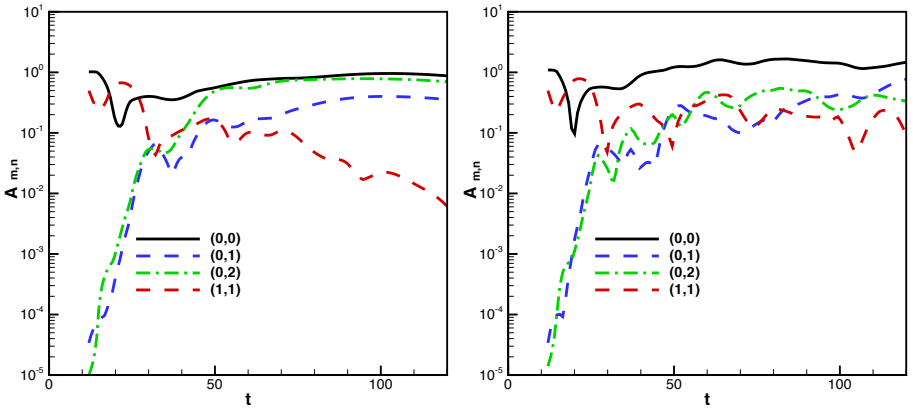

(a) (b)

FIGURE 11. Variation in time of the amplitude of the different modes extracted by Fourier transform of the velocity snapshots obtained by DNS initialized with the weakly nonlinear solutions at $t = 15$, $\epsilon = 0.0151$ (a) and $\epsilon = 0.0152$ (b). The legend indicates the streamwise and spanwise wavenumbers, as multiples of the α and β values chosen for the optimisation.

order to investigate the mechanisms suddenly leading the optimal perturbation towards a self-sustained state, we have performed a spatial Fourier transform of the streamwise disturbance velocity on the $y = -0.4$ plane, at each 2.5 time units (by selecting a different wall-normal position or variable the results change but marginally). We have tracked the development in time of modes having different wavenumbers, using their amplitudes $A_{m,n} = \sqrt{\Re(\tilde{u}_{m,n})^2 + \Im(\tilde{u}_{m,n})^2}$. The Fourier amplitudes of the most relevant modes, normalized with respect to the initial amplitude of the mode $A_{0,0}$, are provided in Figure 11 for $\epsilon = 0.0151$ and 0.0152. The mode $(1, 1)$, corresponding to the oblique wave, is represented by a dashed red line, the mean flow deformation $(0, 0)$ is given by the solid line, and streaky structures, $(0, 2)$ and $(0, 1)$ by the blue and green lines. For the lower

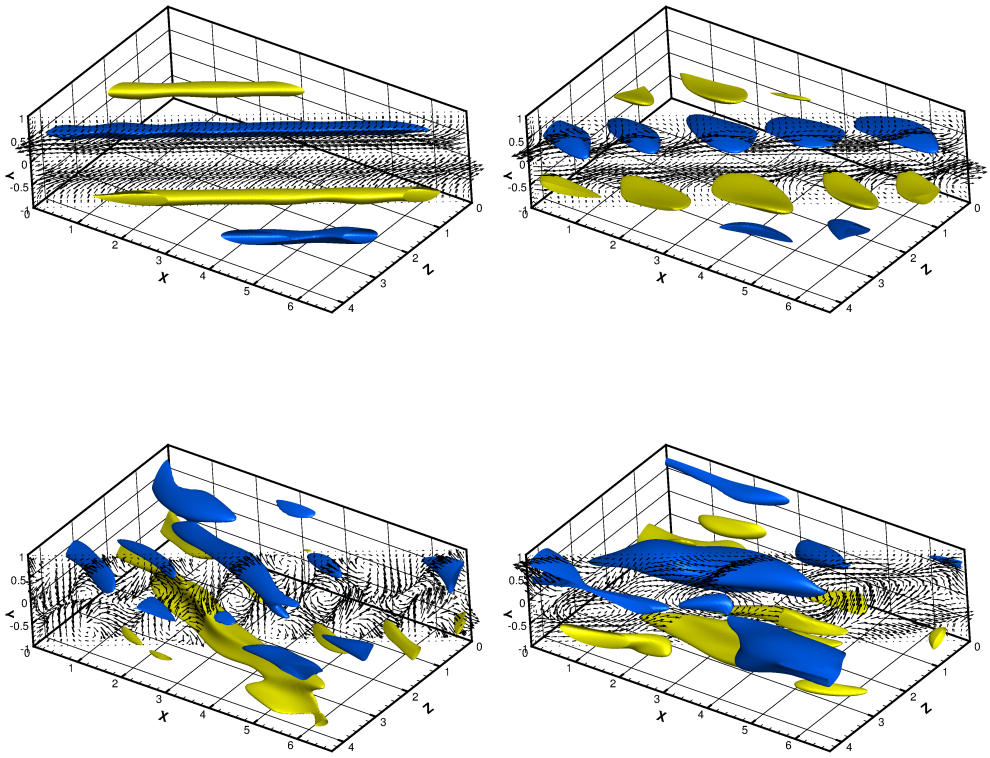

FIGURE 12. Isosurfaces of the streamwise perturbation to the base flow (yellow and blue for $u = \pm 0.3$, respectively), extracted from a DNS initialized with the optimal solution at $t = 15$ for $\epsilon = 0.0152$. The snapshots are extracted at $t = 25, 30, 35, 45$.

value of ϵ the scenario appears similar to the early phases of oblique transition. At the initial time of the DNS ($t = 15$), the flow is composed by the wavy disturbance and its corresponding mean flow deformation. While the energy of the former decreases in time, the latter increases and saturates towards an almost steady state; at the same time, streaky modes begin to be generated from the initial numerical noise, and slowly saturate in time. However, the amplitude of the induced mean flow distortion is not sufficiently high to sustain a regeneration cycle cycle, and after a long saturation phase, the streaks decay towards the laminar state (frame (a) of figure 11). On the other hand, when ϵ is slightly larger, the self-sustained cycle is triggered very suddenly, roughly after 10 time units. As one can observe in frame (b) of figure 11, the streaky modes generated by the initial noise do not experience the slow phase of saturation and secondary instability observed in the classical bypass transition scenario, but they rapidly reach a chaotic dynamics. This behaviour is not surprising, since the perturbation has been optimized by taking into account non-linear effects; thus, it should be able to skip some of the linear phases of growth of the perturbations, similarly to fully non-linear optimals (cf., for instance, Cherubini *et al.* (2011)).

The different phases of the weakly non-linear optimal transition are displayed in figure 12 where isosurfaces of the streamwise perturbation are plotted together with velocity

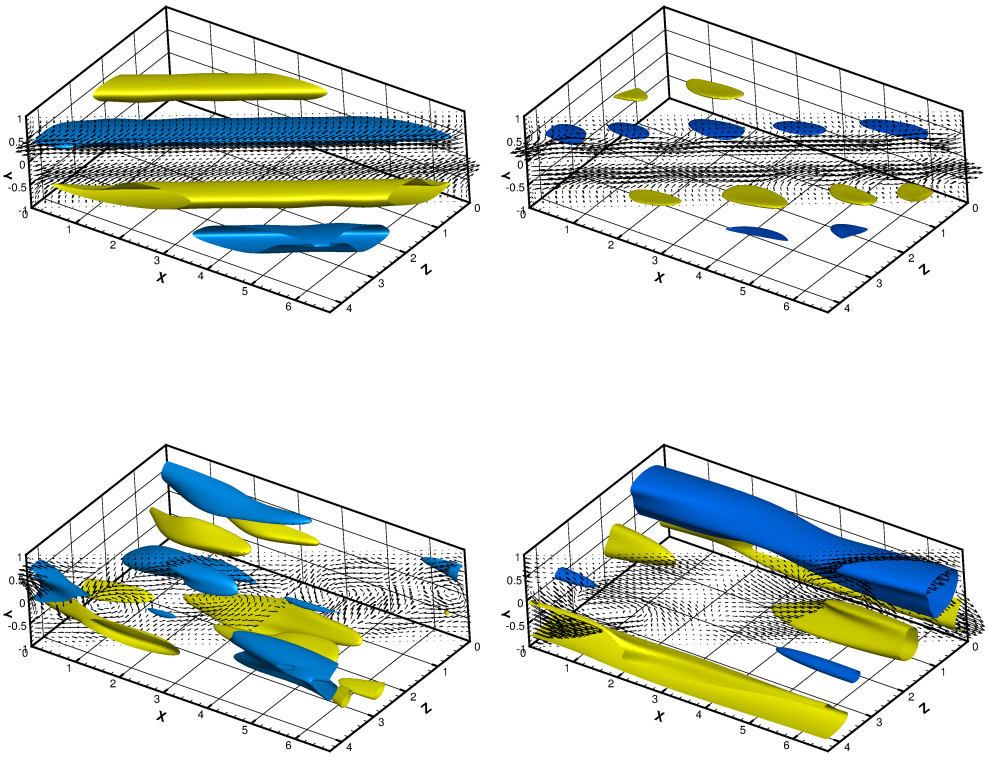

FIGURE 13. Isosurfaces of the streamwise perturbation to the base flow (yellow and blue for $u = \pm 0.2$, respectively), extracted from a DNS initialized with the optimal solution at $t = 15$ for $\epsilon = 0.0151$. The snapshots are extracted at $t = 25, 30, 45, 75$.

vectors in a plane parallel to the direction of the oblique wave. At $t = 25$ (first frame), the mean flow distortion has induced an inflectional region at $y \approx 0$. The inflectional instability triggered in this region produces an array of vorticity rolls normal to the direction of the oblique wave (second frame). The rolls increase in amplitude, transporting the base flow momentum, creating inclined zones of strong high and slow streamwise velocity (third frame). It is noteworthy that the presence of inclined rolls and low- and high-momentum regions is a key feature found in fully non-linear optimal perturbations in Couette flow (see Monokrousos *et al.* (2011); Rabin *et al.* (2012); Cherubini & De Palma (2013)). Finally, after 55 time units, these chaotic structures lose memory of the initial inclination provided by the vortices, and a self-sustained chaotic motion is observed. On the other hand, for a lower value of ϵ, although similar structures are created at early times, they are not able to self-sustain. Figure 13 shows that, after 30 time units, rolls of vorticity normal to the direction of the oblique wave begin to be generated. However, their amplitude being too weak, they cannot be sustained in time by non-linear effects; thus, they begin to decay. During this slow decay phase, the streamwise vorticity component of those rolls slowly begin to generate streamwise streaks, which can be observed in the fourth frame of figure 13. However, since the regeneration cycle is not sustained due to the weak effect of non-linearities, the streaks saturate and then slowly decay.

The trajectory of the flow in these two cases can be observed on a projection of the phase space given by the energy input rate, I, and the integral dissipation rate, D, normalized by their respective laminar values and defined as:

$$I = \frac{\alpha_{opt}\beta_{opt}}{4\pi^2}\int_0^{2\pi/\alpha_{opt}}\int_0^{2\pi/\beta_{opt}}\frac{1}{2}\left[\left(\frac{\partial u}{\partial y}\right)_{y=-1}+\left(\frac{\partial u}{\partial y}\right)_{y=1}\right]dx\,dz, \tag{4.2}$$

$$D = \frac{1}{V}\int_0^{2\pi/\alpha_{opt}}\int_{-1}^{+1}\int_0^{2\pi/\beta_{opt}}|\boldsymbol{\omega}|^2\,dx\,dy\,dz, \tag{4.3}$$

where $\boldsymbol{\omega}$ represents the vorticity vector. This projection of the phase space (see, e.g. Kawahara & Kida (2001)) allows to visualize the balance between the energy injected in the system through the moving walls and that dissipated by viscosity in the whole domain. As discussed by Kawahara & Kida (2001), the laminar attractor sits in the point $I = D = 1$; the turbulent statistically stationary state is close to $I = D \approx 3$, whereas all other equilibrium solutions are situated on the $I = D$ diagonal, indicated in the two frames of figure 14 by dashed lines. As shown in figure 14 (a), the trajectories start from the upper left part of the plane (the empty triangles indicating the starting point of the trajectory and its direction), corresponding to an energy input very close to the laminar one and a rather high dissipation value. This is not surprising since the initial flow structures are not placed close to the wall, where energy enters the system, but rather around the center of the domain in $y = 0$. The light blue trajectory shows that, for $\epsilon = 0.0151$, after a rapid decrease of the dissipation, the trajectory bends towards the $I = D$ bisector, locus of equilibrium solutions. However, the perturbation amplitudes reached are not sufficiently high to escape from the laminar attractor. On the other hand, for $\epsilon = 0.0153$, the trajectory spends much time close to the bisector, and then leaves towards higher values of the energy input and dissipation rate, which are characteristic of the turbulent dynamics. The slow-down of the trajectory in correspondence of the bisector, in a region characterized by I and D values intermediate between the laminar and the turbulent ones, might be the signature of the passage of the perturbation close to a relative attractor on the laminar-turbulent boundary (the edge state, see Schneider *et al.* (2008); Schneider & Eckhardt (2006); Skufca *et al.* (2006)). Indeed, for an initial amplitude far from the laminar-turbulent boundary, $\epsilon = 0.0157$ (green line), the trajectory does not pass close to the bisector before reaching turbulence, but displays strong values of D, typical of a bursting phenomenon (see also van Veen & Kawahara (2011); Cherubini & De Palma (2013)).

Finally, in order to evaluate the efficiency of the weakly non-linear optimal perturbations in inducing turbulence, we have compared these trajectories with those followed by a linear optimal perturbation, computed for the same target time. The linear optimal perturbation has been rescaled in amplitude in order to have at $t = 15$ the same integral energy of the weakly non-linear solutions for $\epsilon = 0.0151$ and 0.0157. The light blue and green curves in figure 14 (b) show that, for these amplitudes, the linear optimal perturbation is not able to induce transition, but rather leads to very fast relaminarization. Increasing the initial energy of these perturbations by 5 times still does not lead the flow to transition (as shown by the red line in figure 14 (b)), but rather induces a strong bursting event which slowly decays in time. Thus, we can conclude that weakly non-linear optimal perturbations are indeed more effective in inducing transition than linear ones.

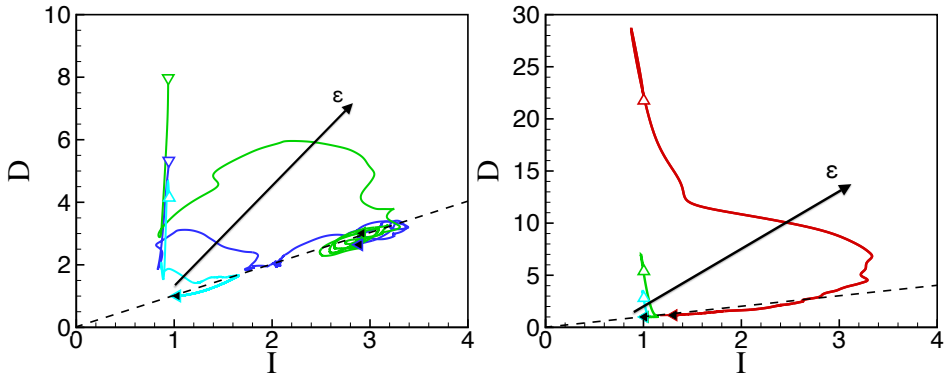

FIGURE 14. Trajectories on a $I - D$ projection of the phase space of the (a) weakly non-linear optimal solutions obtained for $\epsilon = 0.0151, 0.0153, 0.0157$ and (b) of the corresponding linear optimal solutions rescaled with increasing amplitudes. Note that the arrows indicate increasing values of ϵ. The starting points of the trajectories, as well as their direction, are indicated by the white triangles, whereas the full triangles indicate the ending points.

5. Conclusions

A formulation of the optimal-perturbation problem in shear flows is proposed, which takes into account the distortion of the base flow by the action of the Reynolds stresses, modeled by averaging the products of single-mode disturbance waves. The technique proposed permits to consider the effect of the amplitude ϵ of the initial disturbance field and to isolate a strongly receptive region of wavenumber space, for T sufficiently small for the theory to remain tenable, which differs significantly from the most selective range of linear optimal disturbances.

The simplicity of the weakly nonlinear model permits to compute thresholds separating initial states which relaminarize from those which grow without bound, in a fraction of the time compared to full DNS and thereby the model represents a valuable tool for parametric studies of the early stages of the laminar–turbulent transition. The importance of including the spanwise mean-flow distortion terms in the equations describing the transient amplification of oblique flow structures has been demonstrated: although the $\epsilon^2 w_{00}$ terms are small in magnitude their influence on the cross-stream terms in the wave equations is not negligible.

It would, however, be illusory to expect for the present highly truncated model to yield accurate transition thresholds, since transition relies on the growth and interaction of several modes. We have thus performed Direct Numerical Simulations to unravel the transition scenarios induced by the weakly nonlinear optimal disturbances. Concerning the energy amplification, a remarkable agreement is found between the DNS and the weakly nonlinear model results, for initial amplitudes below threshold. For larger amplitudes, non-linear effects become too strong to be correctly captured by a weakly non-linear expansion. However, when $\epsilon \geqslant \epsilon_{crit}$, the optimal perturbation resulting at finite time from the weakly non-linear model is able to induce a self-sustaining cycle leading to turbulence, whereas a linear optimal disturbance computed for the same target time leads to relaminarization, even when the initial energy is rescaled to very large values. The self-sustained cycle identified is triggered by an inflectional instability at the center of the domain, resulting from the mean flow distortion induced by Reynolds

stresses. This inflectional instability generates an array of vorticity rolls in the direction normal to the oblique wave, that, while increasing in amplitude, transport the base flow momentum, creating inclined zones of high and low streamwise velocity. Finally, these chaotic structures lose memory of the initial inclination provided by the vortices, and sustained chaotic motion is observed.

The financial support to the PRIN 2012 project, no. D38C1300061000, from the Italian Ministry of Education is gratefully acknowledged.

REFERENCES

Andersson, P., Berggren, M. & Henningson, D.S. 1999 Optimal disturbances and bypass transition in boundary layers. *Physics of Fluids* **11** (1), 134–150.

Andersson, P., Brandt, L., Bottaro, A. & Henningson, D. S. 2001 On the breakdown of boundary layer streaks. *Journal of Fluid Mechanics* **428**, 29–60.

Beaume, C., Chini, G. P., Julien, K. & Knobloch, E. 2015 Reduced escription of exact coherent states in parallel shear flows. *Phys. Rev. E* **91**, 043010.

Biau, D. & Bottaro, A. 2009 An optimal path to transition in a duct. *Phil. Trans. R. Soc. A* **367**, 529–544.

Blackburn, H. M., Hall, P. & J., Sherwin S. 2013 Lower branch equilibria in coeutte flow: the emergence of canonical states for arbitrary shear flows. *Journal of Fluid Mechanics* **R2**, 726.

Bottaro, A., Soueid, H. & Galletti, B. 2006 Formation of secondary vortices in turbulent square-duct flow. *AIAA Journal* **44** (4), 803–811.

Butler, K.M. & Farrell, B.F. 1992 Three-dimensional optimal perturbations in viscous shear flow. *Physics of Fluids A* **4** (8), 1637–1650.

Cherubini, S. & De Palma, P. 2013 Nonlinear optimal perturbations in a Couette flow: bursting and transition. *Journal of Fluid Mechanics* **716**, 251–279.

Cherubini, S., De Palma, P., Robinet, J.-C. & Bottaro, A. 2011 The minimal seed of turbulent transition in the boundary layer. *Journal of Fluid Mechanics* **689**, 221–253.

Corbett, P. & Bottaro, A. 2001 Optimal linear growth in swept boundary layers. *Journal of Fluid Mechanics* **435**, 1–23.

Cousteix, J. & Mauss, J. 2007 *Asymptotic Analysis and Boundary Layers*. Springer-Verlag, Berlin.

Criminale, W.O., Jackson, T. L., Lasseigne, D.G. & Joslin, R.D. 1997 Perturbation dynamics in viscous channel flows. *Journal of Fluid Mechanics* **339**, 55–75.

Duguet, Y., Monokrousos, A., Brandt, L. & Henningson, D.S. 2013 Minimal transition thresholds in plane Couette flow. *Physics of Fluids* **25** (8), 084103.

Farrell, B.F. & Ioannou, P.J. 2012 Dynamics of streamwise rolls and streaks in turbulent wall–bounded shear flow. *Journal of Fluid Mechanics* **708**, 149–196.

Gatti, D. & Quadrio, M. 2013 Performance losses of drag-reducing spanwise forcing at moderate values of the Reynolds number. *Physics of Fluids* **25**, 125109.

Gustavsson, L. H. 2009 Non-linear wave interactions from transient growth in plane-parallel shear flows. *European Journal of Mechanics - B/Fluids* **28** (3), 420 – 429.

Hall, P. & Sherwin, S. J. 2010 Streamwise vortices in shear flows: harbingers of transition and the skeleton of coherent structures. *Journal of Fluid Mechanics* **661**, 178–205.

Kawahara, G. & Kida, S. 2001 Periodic motion embedded in plane Couette turbulence: regeneration cycle and burst . *J. Fluid Mech.* **449**, 291–300.

Landahl, M. 1975 Wave breakdown and turbulence. *SIAM Journal on Applied Mathematics* **28** (4), 735–756.

Luchini, P. 2000 Reynolds-number-independent instability of the boundary layer over a flat surface: optimal perturbations. *Journal of Fluid Mechanics* **404**, 289–309.

Luchini, P. & Bottaro, A. 2014 Adjoint equations in stability analysis. *Annual Review of Fluid Mechanics* **46** (1), 493–517.

Monokrousos, A., Bottaro, A., Brandt, L., Di Vita, A. & Henningson, D.S. 2011

Nonequilibrium thermodynamics and the optimal path to turbulence in shear flows. *Phys. Rev. Lett.* **106**, 134502.

Pringle, C.C.T. & Kerswell, R.R. 2010 Using nonlinear transient growth to construct the minimal seed for shear flow turbulence. *Phys. Rev. Lett.* **105**, 154502.

Pringle, C.C.T., Willis, A.P. & Kerswell, R.R. 2012 Minimal seeds for shear flow turbulence: using nonlinear transient growth to touch the edge of chaos. *Journal of Fluid Mechanics* **702**, 415–443.

Rabin, S. M. E., Caulfield, C. P. & Kerswell, R.R. 2012 Triggering turbulence efficiently in plane Couette flow. *J. Fluid Mech.* **712**, 244–272.

Schmid, P.J. & Henningson, D.S. 1992 A new mechanism for rapid transition involving a pair of oblique waves. *Physics of Fluids A* **4** (9), 1986–1989.

Schmid, P.J. & Henningson, D.S. 2001 *Stability and Transition in Shear Flows. Applied Mathematical Sciences* v. 142. Springer New York.

Schneider, T. M. & Eckhardt, B. 2006 Edge of chaos in pipe flow. *Chaos* **16** (4), 041103.

Schneider, T. M., Gibson, J. F., Lagha, M., De Lillo, F. & Eckhardt, B. 2008 Laminar-turbulent boundary in plane Couette flow . *Phys. Rev. E* **78**, 037301.

Skufca, Joseph D., Yorke, James A. & Eckhardt, Bruno 2006 Edge of chaos in a parallel shear flow. *Phys. Rev. Lett.* **96**, 174101.

Van Dyke, M. 1975 *Perturbation Methods in Fluid Mechanics*. The Parabolic Press, Stanford, CA.

van Veen, L. & Kawahara, G. 2011 Homoclinic tangle on the edge of shear turbulence . *Phys. Rev. Lett.* **107**, 114501.

Verzicco, R. & Orlandi, P. 1996 A finite-difference scheme for three-dimensional incompressible flows in cylindrical coordinates. *Journal of Computational Physics* **123** (2), 402–414.

Zuccher, S., Bottaro, A. & Luchini, P. 2006 Algebraic growth in a Blasius boundary layer: Nonlinear optimal disturbances. *European Journal of Mechanics - B/Fluids* **25** (1), 1 – 17.